Efficient computation and experimental validation of ACSR overhead line conductors under tension and bending

R. Baumann*[1] and P. Novak[2]

Abstract:

The paper revisits an important subject in the field of conductor inner mechanics, i.e. the bending behavior of overhead line conductors under tension. It proposes an efficient Finite Element Model based on beam elements for the individual conductor wires and compares the simulation results with existing theoretical models but also with extensive measurements in a purpose-made test rig. Both comparisons show a very satisfactory correlation and encourage for a wide application of this FE model.

1. Introduction

Overhead line conductors may look simple, but are in reality complex spiral structures, which mechanical behavior is not yet fully understood. Particular effort has been given in the past in the bending process of conductors under axial loads, since this is the basis for understanding the conductor behavior under variable, dynamic loads, as those caused by wind induced, so called Aeolian vibrations, which may lead to fatigue failures, [1]. A core issue in this respect is the conductor bending stiffness, as it influences the deflection and subsequently the wire strains (or stresses) of the conductor. Quite a few models have been proposed in the past for the bending stiffness, an excellent summary been given in [2]. Many refer to [3] for a comprehensive description of the physical behavior of a conductor during bending and use the measurements reported in [3] and [4] for validation [5]. In this sense a major contribution of the present paper is to repeat similar experiments with those in [4], with another frequently used conductor (ACSR Drake) and also applying a different measuring technique. Another important contribution of this paper is to propose an efficient Finite Element modeling technique, i.e. by using beam elements for the individual conductor wires instead of full 3D solid elements. This enables conductor bending simulations within a realistic time frame and hardware usage.

2. Spiral Rope Mechanics

An overhead line conductor is in terms of wire rope terminology a spiral rope. It consists of a number of round wires which are placed in different layers over the core wire; these layers have in the case of overhead line conductors an alternate lay angle, Fig. 1. Often the core wire and the first (or even the second layer) is made of steel, while the outer layers are made from aluminum and its alloys.

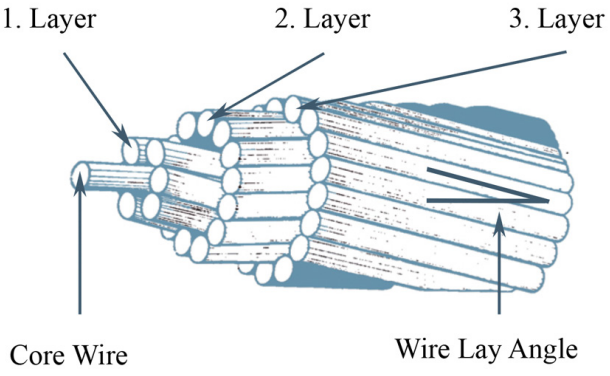

Fig. 1. Principal layout of an overhead line conductor.

Conductors are in first place loaded under tension caused by their own weight and external loads such as wind and ice. In addition they see - mainly at their suspension points - static as well as alternating bending loads, the latter caused by wind-induced, so called Aeolian vibrations. These loads are shown schematically in Fig. 2.

1- R. Baumann* is with the Competence Center Mechanical Systems, Lucerne University of Applied Sciences and Arts, Horw, 6048, Switzerland (e-mail: ralf.baumann@hslu.ch, see http://www.hslu.ch/ccms).

2- P. Novak was at the time of the project with the Competence Center Mechanical Systems, Lucerne University of Applied Sciences and Arts, Horw, 6048, Switzerland.

KEYWORDS

Conductor, Hysteresis, Finite Element Analysis, Overhead Line, Tests

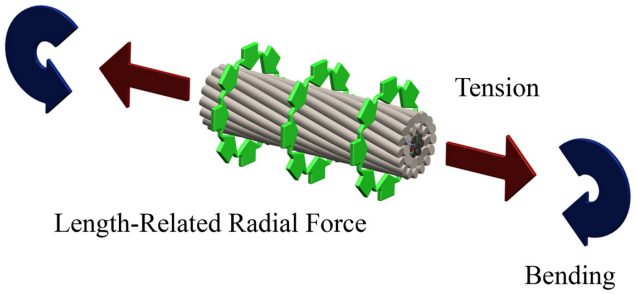

Fig. 2. Loads acting on a conductor.

Above mentioned loads have to be shared by the individual conductor wires; this is shown for a piece of a wire in Fig. 3. When the wire is loaded in tension, the radius of the wire helix is decreased causing torsional and bending stresses. This decrease introduces a radial compression on the underlying wires. When now by external influences such as alternating bending, the wires tend to move, this movement is counterbalanced by the inter-wire friction, which causes an additional normal stress on the wire cross-section. This process has been described in [4].

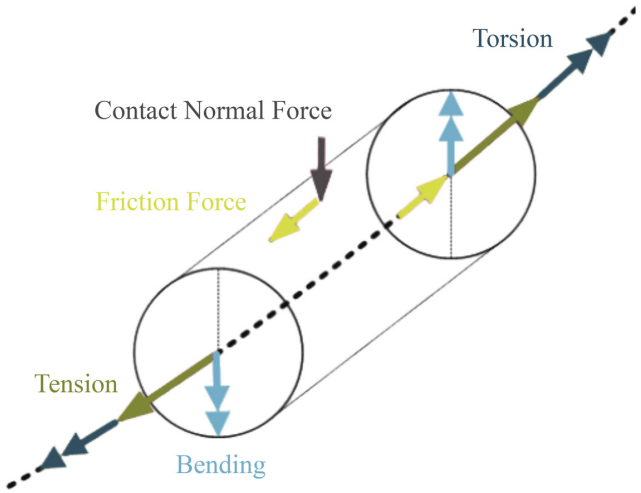

Fig. 3. Loads acting on a conductor wire.

From the above can be concluded that the bending stiffness of a conductor is not constant, as in a beam with uniform cross-section, but depends on the displacements of the individual conductor wires, i.e. whether they are in the stick or the slip state, as explained in [4]. The theoretical relationship of the bending stiffness to the curvature for an ACSR Drake conductor (ACSR - Aluminum Conductor Steel Reinforced), examined in this paper, is shown in Fig. 4 for a tension of 28.5 kN. The theoretical upper limit of the bending stiffness EI_{max} is based on the assumption that all wires are 'glued' together and no slip exists. The lower limit EI_{min} is characterized by a state with no interaction between the individual wires.

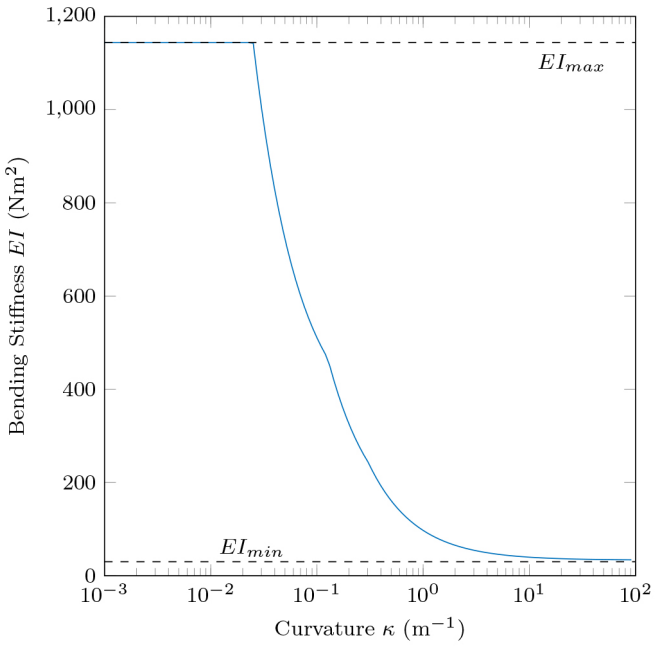

Fig. 4. Theoretical relationship of the bending stiffness to the curvature for ACSR Drake at a tension of 28.5 kN.

3. Conductor FEM Model

Advances in FEM simulations and the dramatic increase in computational power of hardware enabled the application of FEM also to conductors, despite their complex structure and geometry. A special challenge poses the proper modeling of the inter-wire contacts and the related frictional effects.

The simplest FEM model is a so-called continuum model, i.e. the conductor is replaced by a cylindrical body with 'smeared' orthotropic material properties, [6], Fig. 5a. In this case it is not possible to represent adequately the inter-wire contacts, which are of great importance for a realistic simulation. On the other end of modeling complexity is the implementation of a volume based model, Fig. 5b, where all individual wires are discretized by solid elements [7]. This approach allows the proper representation of the inter-wire contacts, but reaches

easily, even at moderate FEM mesh densities, a very high number - in the millions range - of DOF (degrees of freedom). This leads consequently to unacceptable high computational costs, even at high performance hardware platforms. Most of the published models are restricted in terms of conductor length and number of layers. Additionally the applicable loads are very often limited to tension and torsion. To simulate a bending load case for a conductor more than 0.5 m long and with more than two layers is still a challenging task.

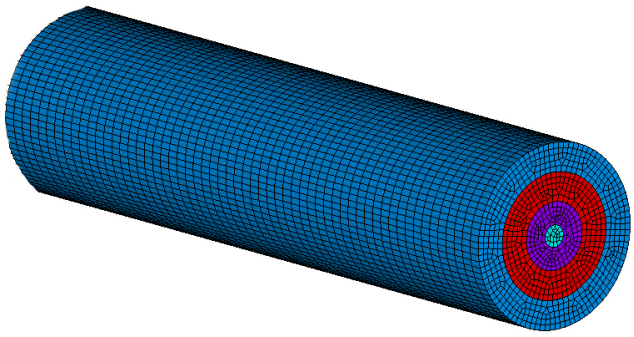

(a) Continuum model

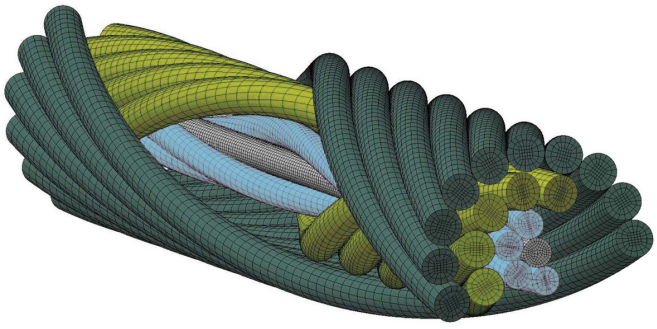

(b) Solid model

Fig. 5. Two different approaches of FEM conductor volume models.

A more efficient approach is the modeling of the individual wires as beam elements, Fig. 6, [8], [9], [10] and [11]. This allows, with a reasonable number of DOF, the simulation of all wire loads, such as tension, compression, bending and torsion. In addition it is possible to implement a parametric modeling approach easily, since all nodes are located on a helix, which can be perfectly described mathematically.

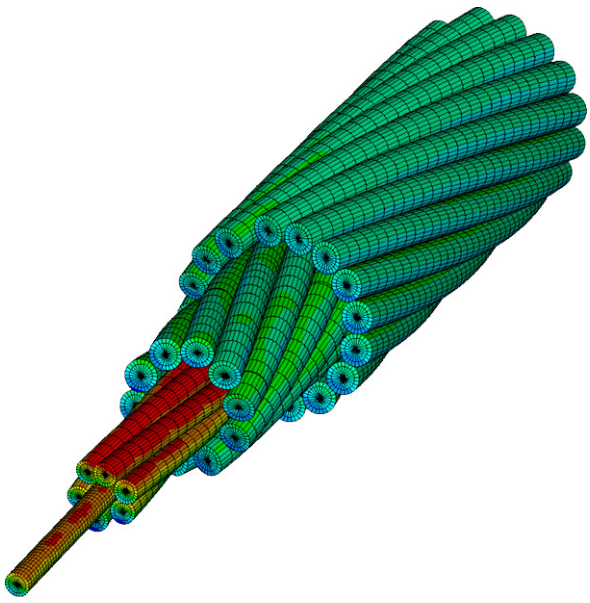

Fig. 6. FEM beam conductor model.

The modeling of the inter-wire contacts plays, as mentioned above, a key role in the whole modeling process. The contact situation in a conductor is shown schematically in Fig. 7. The axial wire loads (tension) cause compressive loads on the underlying wires, creating point inter-wire contacts in radial direction. Rarely and depending on wire size and conductor geometry (e.g. diameter and lay angle) wires of the same layer 'touch' each other in so-called line contacts in hoop direction.

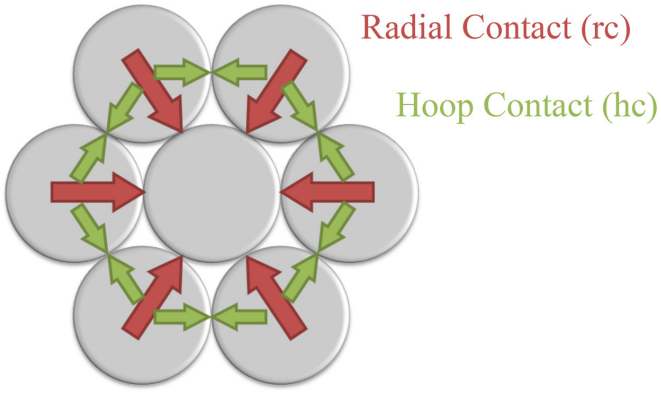

Fig. 7. Contact situation in a simple 1+6 conductor.

The numerical modeling and study is done with the ANSYS APDL code. Therefore a graphical user interface (GUI) based on MATLAB is developed, which easily allows setting all relevant conductor parameters and the generation of the APDL input deck, Fig. 8.

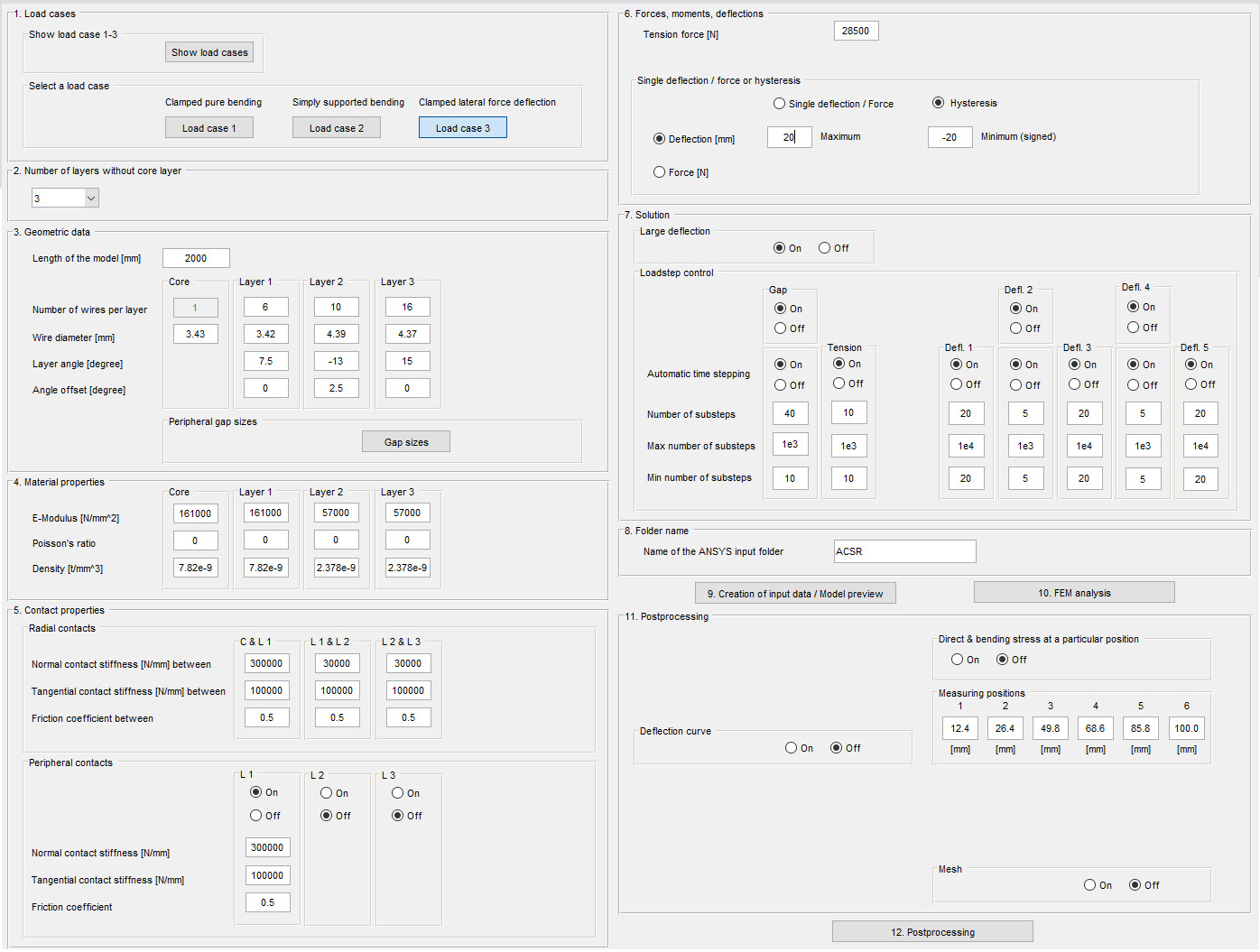

Fig. 8. Graphical user interface for model setup.

Because the effects of torsion moments resulting from friction have not been taken into account, an approach with classical gap elements was chosen instead of using the ANSYS standard beam contact elements. The setup of the mesh is basically driven by the positon of the contact points of the crossing wires, with the exception of the first layer, where an equidistant node distribution is being applied for contacting the core wire. Based on the conductor geometric parameters, the contact points, whose positions can be computed precisely in advance, define also the position of the beam center nodes.

The contact gap elements are created by inserting two additional nodes at the geometric contact point between two wire elements. These pivot nodes ensure the proper consideration of out-of-center forces, like friction loads, and the respective torques on the wires. They are subsequently connected with the central nodes of the related beam elements by suitable constraints called rigid links, Fig. 9. The contact elements are based on a penalty algorithm. This allows by predefined normal and tangential contact stiffness to adequately consider the contact and wire compliance in radial direction, as well as tangential forces caused by Coulomb friction. For a first estimation of the contact stiffness, the well-known formulas from Hertz [12] are used. By conducted parameter studies, the following values have turned out to be a good compromise between convergence behavior and allowable penetration rate: $3 \cdot 10^8$ N/m in normal direction for the contact between core and first layer, $3 \cdot 10^7$ N/m in normal direction for all crossing contacts, 10^8 N/m in tangential direction. The friction coefficient of 0.5 is taken from the experiments reported in [3]. The same approach is used for the modeling of the hoop contacts, whereby equidistant nodes between two neighbor wires simulate the line contact.

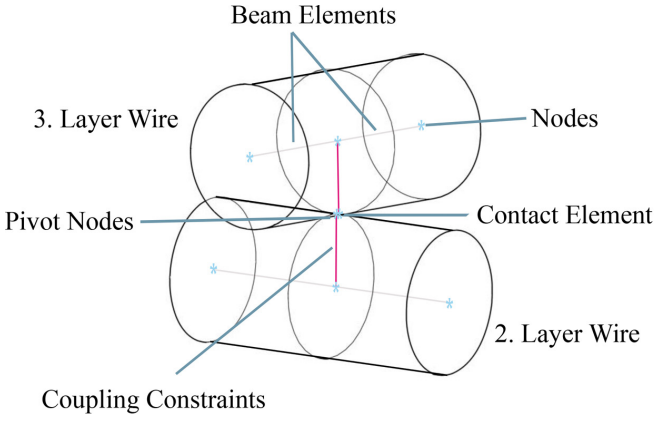

Fig. 9. Contact modeling shown for two beam elements.

At both ends of the conductor FEM model, the end nodes of the beam elements are all connected by rigid links to the master nodes, which are usually the end nodes of the core beam elements. On these master nodes, the corresponding boundary conditions are applied: simply supported or clamped, depending on the case under consideration. Loads are also applied on these nodes, i.e. point force for tension and bending moments in the case of stiffness/curvature studies.

Depending on the conductor type and geometric parameters, hoop contacts have to be taken into account. In general the consideration of hoop contacts lead to higher number of elements and nodes. Fig. 10 and 11 show two different models of a 3-layer conductor (ACSR Drake). The first mesh is generated including hoop contacts in each layer, the second mesh only for the first layer. The user can decide in which layers hoop contacts should be applied (GUI). As the application of hoop contacts in all layers can double the size of DOF, a specific selection is useful. The gap size between single wires in hoop direction can easily computed based on the conductor geometric parameters. The GUI is supporting such calculations. For the ACSR Drake example, hoop contacts can only occur in the first layer.

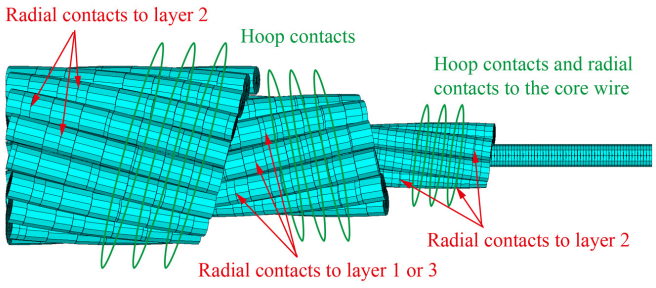

Fig. 10. ACSR Drake mesh with hoop contacts in each layer.

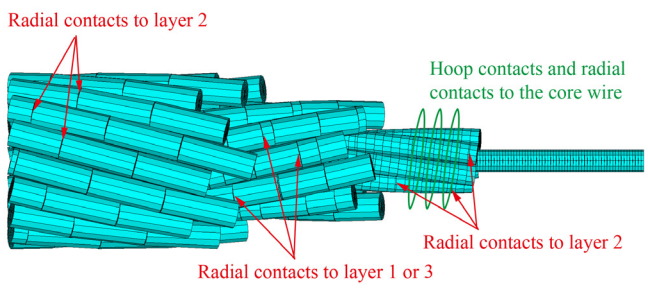

Fig. 11. ACSR Drake mesh with hoop contacts only in the first layer.

As the node positions of the beam elements are given by the contact points, the models do not have a uniform mesh. Especially the outer layers have very high element sizes compared to the core elements. A series of simulations were performed to study the influence of additional mesh refinements on the results, with no significant effects. For the ACSR Drake conductor model the beam element sizes range from 0.4 mm for the core up to 11.9 mm for the outer layer.

An important prerequisite for the proper contact modeling is the assumption of small displacements. Separately conducted simulations have shown that this is a reasonable hypothesis. For example, the simulation of a 2 m 3-layer conductor, with a mid-span deflection of 20 mm, shows a maximum relative displacement, i.e. tangential sliding distance of the two contact points, of approx. 0.6 mm. This is less than 20% of the smallest wire diameter.

The modeling approach presented here is still leading to a model size of approx. 0.4 million DOF for a 2 m 3-layer conductor, including more than 21,000 beam and approximately the same number of contact elements (including hoop contacts only for the first layer). For a 5-layer conductor the DOF can easily reach two millions. The computation times for quasi-static, non-linear simulations on state-of-the-art PC hardware varies between minutes and hours, depending on the size of the model and the simulation task. In this study several simulations were conducted, starting with simple tension loadings for different lengths up to full cyclic transverse loading to determine hysteresis curves. For example doing a simple deflection analysis on a 3-layered, 2 m long conductor the computation time on a notebook (i7-6820 HQ @ 2.7 GHz, 16 GB RAM) running on 4 cores takes about 45 minutes. An entire hysteresis cycle takes about 100 minutes.

4. Experiments

The test arrangement, Fig. 12, basically follows the proposal in [3] and [4], whereby here the conductor length has been selected to be 2 m, in order to simplify the measurement procedure and to minimize possible influences from the end fixations. The experimental set-up was designed to measure deformations and wire stresses.

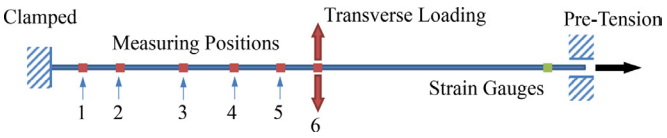

Fig. 12. Schematic of test bench.

For the tests an ACSR Drake has been used, as one of the most commonly used conductors in related literature. Drake has a (1 + 6) wire steel core, with two layers (10 + 16) of aluminum wires. The conductor outer diameter measures approx. 28 mm, Fig. 13. Detailed material and geometric properties are given in Table I. The wire diameters as well as the Modulus of Elasticity were measured over a series of test specimens. The documented values represent mean values and have been used for the simulation models.

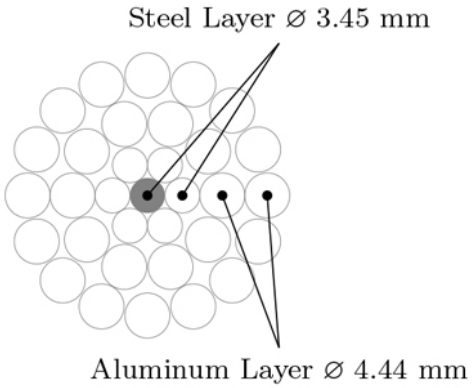

Fig. 13. ACSR Drake conductor.

Table I

Material and geometric properties of the ACSR Drake conductor.

Layer	Wire diameter [mm]	Lay angle [°]	Modulus of Elasticity [GPa]
Core	3.43	-	161
1	3.42	7.5	161
2	4.39	-13	57
3	4.37	15	57

The tested conductor has been clamped at both ends and has been pre-stressed with a hydraulic up to 28.5 kN, a typical tensile load for this conductor. This load has been kept constant during the tests, as the anchoring on one side of the conductor could slide. Conductor bending was introduced by a transverse load applied at the center of the test span. Due to lack of space, the distance between the clamp and the wedge type tension clamp was approx. 0.5 m. Fig. 12 shows the principle, Fig. 14 the test bench as realized.

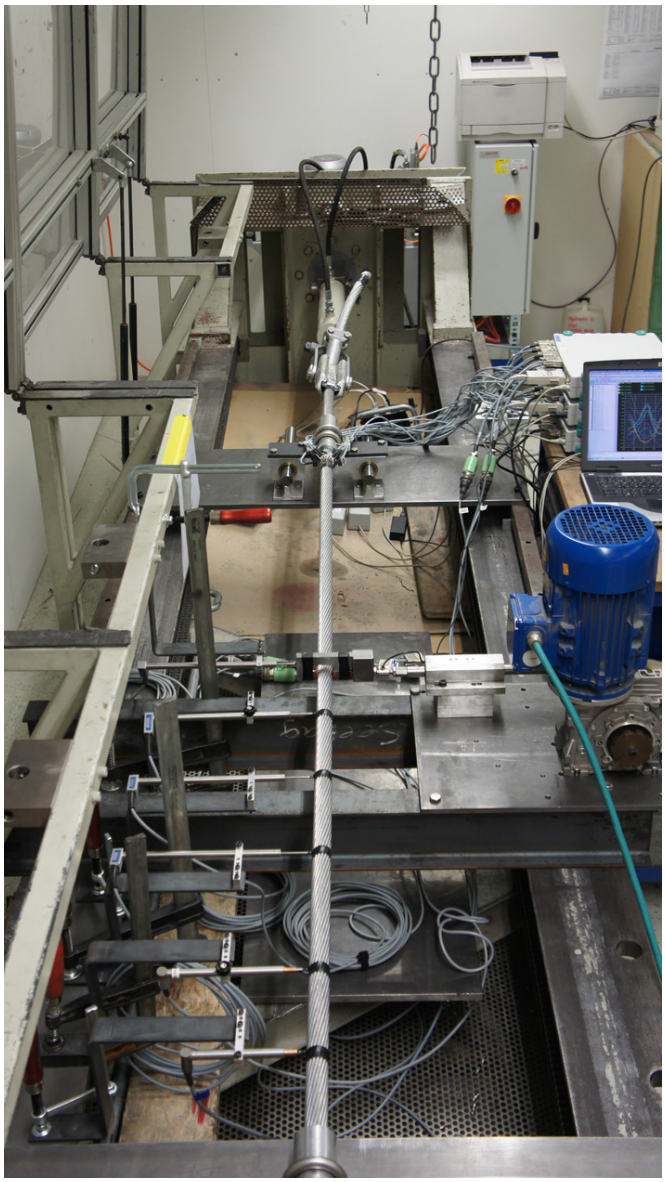

Fig. 14. Test bench with ACSR Drake conductor.

While an electrically driven crank mechanism guarantees for a smooth deflection of the conductor, six displacement sensors, which are applied along the test specimen measure the local deflections. At the same time a force transducer, installed between crank drive and load application, monitors the transverse load applied to the

mid-point of the test sample. Strain gauges applied to all 16 wires of the outer layer close to the sliding fixed end measure and store the related wire strains. This is done over a number of bending cycles, enabling a reasonable averaging of the measured values, which by nature show a statistical spread.

5. Analytical Verification

In this section the simulation results are discussed upon their physical plausibility and compared with the results gained from analytical formulas based upon well accepted rope respectively conductor models [13].

5.1. Comparison of the Wire Tensile Loads

The wire tensile load $Z_{d,L}$ on wire d in layer L can be calculated for the total tensile load S acting upon the conductor using (1) with z_L the number of wires per layer ($L = 0$ for the core wire) and β_L the lay angle, Fig. 15,

$$Z_{d,L} = \frac{\frac{\cos^2 \beta_d}{1 + \nu_d \sin^2 \beta_d} E_d A_d}{\sum_{L=0}^{n} \left(\frac{z_L \cos^3 \beta_L}{1 + \nu_L \sin^2 \beta_L} E_L A_L \right)} S \qquad (1)$$

where

- n number of layers;
- v Poison ratio;
- E Modulus of Elasticity;
- A wire cross section.

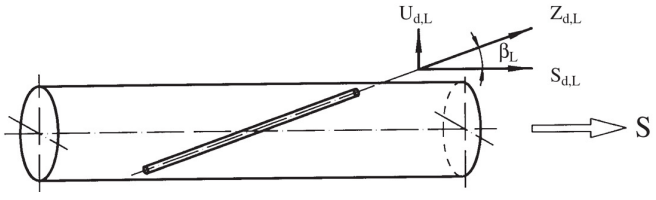

Fig. 15. Decomposition of the tensile load after [3].

The comparison of the wire loads determined analytically with the respective results from the FEM simulation with the beam model is excellent, Table II. The abbreviations 'rc' and 'hc' indicate the contact modes which were taken into account by the simulation: 'rc' means only inter-layer contact (radial) contact, 'rc & hc' mean both radial and contact in the same layer (hoop direction). Hoop contact in conductors is normally non-existent and practically neglected. In the case of ACSR Drake, based on the given geometric properties, only a hoop contact in the first layer theoretically exists. Therefore the model provides a good opportunity to study its influence.

Table II

Wire tension loads [N] at 28.5 kN tension.

Layer	Core	1	2	3
Analytically (1)	1,393	1,361	767	747
FEM (rc)	1,452	1,415	755	730
FEM (rc & hc)	1,312	1,399	769	731

5.2. Comparison of the Contact Forces

Because of the helical wire form, the wire tensions cause compression loads, leading to a distributed radial wire force p_L, where ρ_L is the radius of curvature, Fig. 16.

$$p_L = \frac{Z_{d,L}}{\rho_L} \qquad (2)$$

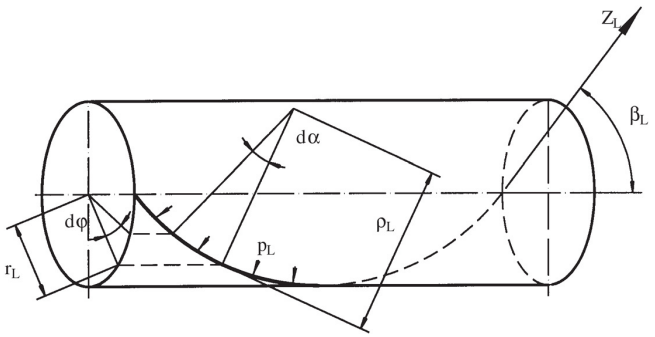

Fig. 16. Length-related radial wire forces ([3], [4]).

Papailiou has shown in [3] and [4], by using (2) and taking into account the geometric relations of a helix, the resultant radial force $N_{d,L}$ of a single wire on the underlying wires can be derived by integration of (3).

$$dN_{d,L} = Z_{d,L} \sin \beta_L d\varphi \qquad (3)$$

To determine the radial normal forces acting on the inner layers, the radial loads from all outer layers, weighted with the relevant number of the layer wires have to be considered. This yields to the following equation for the resultant interlayer radial forces of a single wire d between the first layer and the core wire:

$$N_{d,1-c} = \left(N_{d,3}\frac{z_3}{z_2} + N_{d,2}\right)\frac{z_2}{z_1} + N_{d,1} \qquad (4)$$

Accordingly for the radial force between second and first layer

$$N_{d,2-1} = N_{d,3}\frac{z_3}{z_2} + N_{d,2} \qquad (5)$$

and between third and second layer:

$$N_{d,3-2} = N_{d,3} \qquad (6)$$

These loads act evidently on the crossing points of the wires. For comparison purposes the normal forces at the contact points determined in the FEM simulation are summed up along the conductor. In this case a conductor length of 0.356 m was used. The simulation results are listed in Table III and compared with the analytical values from (4) to (6). For the model neglecting hoop contact, the comparison between the analytical formulas and FEM simulation is very satisfactory, which is understandable as the analytical model does not include effects of hoop contact. For the second case, practically no radial force is acting on the core wire. The interaction of the wires in the steel layer yields a supporting effect, which transfers the loads in circumferential direction, as described in [14].

Table III

Inter radial forces [N] of a single wire (summed-up over 356 mm conductor length) at 28.5 kN tension.

Layer	1 - Core	2 - 1	3 - 2
Analytically (4) – (6)	9,855	4,455	1,575
FEM (rc)	9,374	4,156	1,406
FEM (rc & hc)	≈ 0	4,457	1,516

5.3. Variable Bending Stiffness

The analytical model introduced for the variable bending stiffness in [3] and [4], will be now compared with the FEM simulation using beam elements for an ACSR Drake with 0.356 m length, which will be firstly tensioned and then loaded in bending. Therefore two bending moments were applied at the simply supported ends of the conductor model. From the simulation results the curvature of the core beam element at conductor half-length was derived. The bending stiffness was computed by easily dividing the applied moment by the curvature.

Fig. 17 shows the conductor bending stiffness over the curvature of the conductor axis. The simulations result in a significantly lower bending stiffness in the full stick regime than the analytical model. The latter is based on an ideal assumption that prior to bending all conductor wires fully stick together. It follows that for the calculation of the related bending stiffness Steiner's theorem has to be applied to the moments of inertia of the individual wires as per the following equation [3], [4]:

$$\begin{aligned} EI_{max} &= EI_{min} + EI_{add} \\ &= EI_{min} + \sum_{L=1}^{n}\frac{z_L}{2}r_L^2\cos^3\beta_L\sum_{d=1}^{z_L}E_{d,L}A_{d,L} \end{aligned} \qquad (7)$$

with EI_{add} as the additional bending stiffness term and r_L the radius of each layer.

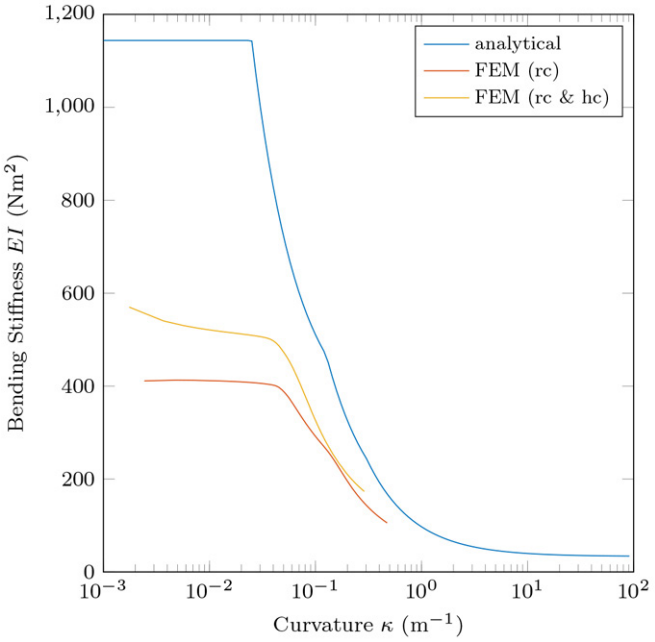

Fig. 17. Comparison of the bending stiffness between FEM simulation with different contact situations and the analytical model from [3] and [4] for 28.5 kN tension.

This approach is based on a number of simplifications. For instance Steiner's terms have to be considered only for those wires which are in contact with another wire in an adjacent layer, as because of manufacturing tolerances and geometric considerations not all wires in a cross-section exhibit necessarily a radial contact. In addition and as explained in [15], the effects of tangential compliance at contact interfaces, which have in reality a finite elliptical shape, should be considered.

The above lead ultimately to a reduction of the theoretical maximum bending stiffness as calculated by (7). This is confirmed by the FEM simulation, which results are shown in Fig. 17. The same figure highlights the stiffening effect of the hoop (line) contacts. In the ACSR Drake conductor examined here such contacts appear only in the first steel layer.

Of interest is also the influence of the conductor tension to the bending stiffness. As analytically shown in [3] and [4] and as intuitively expected, higher tensions delay the wire slip and make thus the conductor stiffer in bending. The FEM simulation results presented in Fig. 18, confirm this relationship.

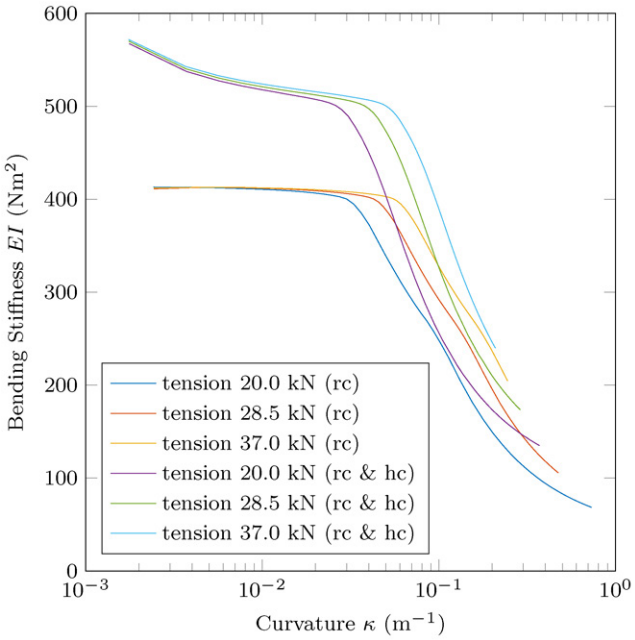

Fig. 18. Comparison of the bending stiffness for different tensions.

5.4. Model Length

Fig. 19 presents the influence of different lengths of the FEM model on the conductor bending stiffness. Simulations with short lengths show significant deviations compared to longer models. For lengths above 0.5 m there is practically no difference between the simulation results. This can be explained through the stiffening effect of the applied boundary conditions, which have a higher influence on shorter conductor lengths.

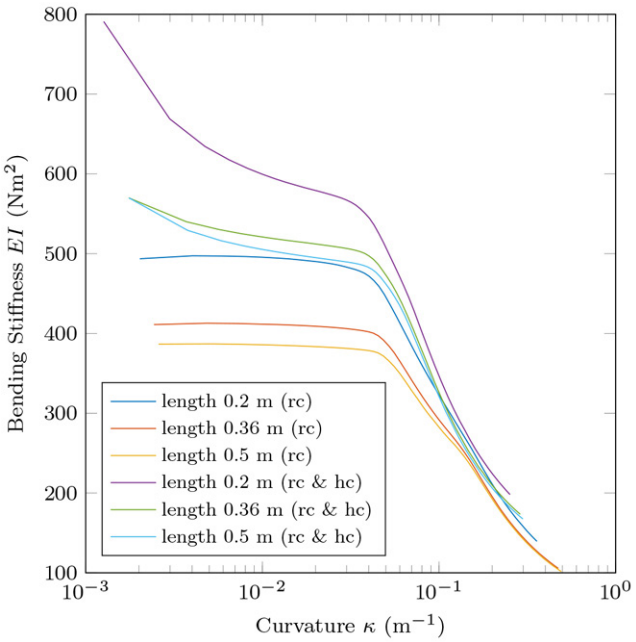

Fig. 19. Comparison of the bending stiffness for different conductor lengths.

6. Experimental Verification

In this section the simulation results are compared with the results gained from experiments. In general all simulations were done by taking into account the hoop contacts. As mentioned before, these contacts do only exists in the first layer for an ACSR Drake conductor. Therefore only those first layer hoop contacts were active.

6.1. Deflection

The comparison between the FEM simulation and the measurements of the conductor deflection on the six locations indicated in Fig. 12 is excellent, Fig. 20. In the same figure are inserted the theoretical deflection curves, in case of constant bending stiffness (EI_{min} and EI_{max}), which emphasizes the distinct influence of the variable bending stiffness. Additionally the deflection curve from the analytical model from Papailiou ([3] and [4]) is given.

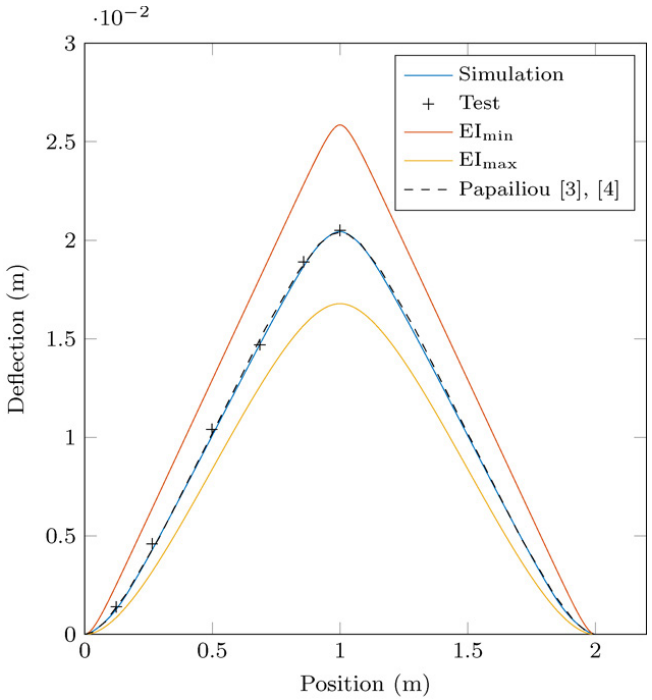

Fig. 20. Comparison between FEM results and tests on the 2 m long ACSR Drake specimen.

6.2. Energy Dissipation

By determining the area covered by the hysteresis it is possible to determine the energy dissipation by friction during bending. This is presented in Fig. 21, where the averaged hysteresis loop at the center of the test sample is shown; its area is a measure for the frictional work. Table IV lists the difference in percentage of the computed frictional work against measurement at six different measuring positions 1 to 6, Fig. 12 and 14. In general the computed dissipation is lower than the measurement results. Interestingly enough, a considerable part of the frictional work is contributed by the hoop contacts between the wires of the same layer. As the value of the friction coefficient contains experimental uncertainties [3], it is possible to reduce the indicated differences by suitably modifying it.

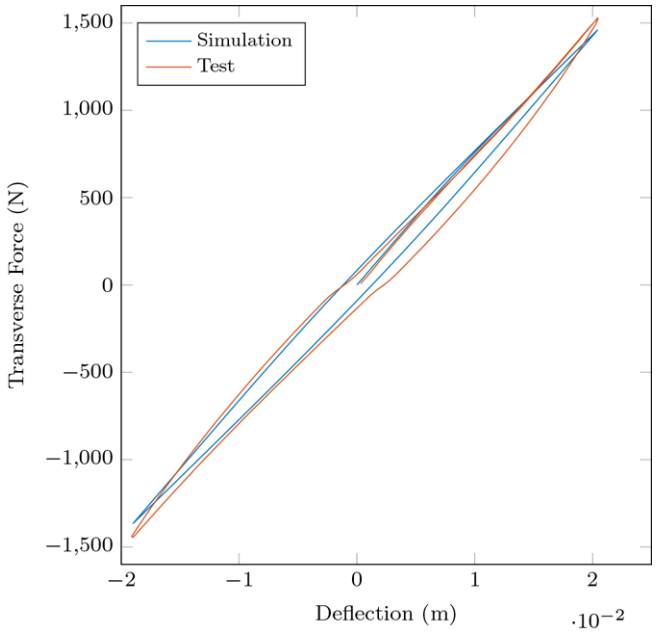

Fig. 21. Hysteresis at mid-span measuring position 6.

Table IV
Measured friction work and difference against simulation results.

Position	1	2	3	4	5	6
Measured friction work [J]	0.73	1.51	2.24	2.89	4.20	4.93
Simulation (rc & hc) [%]	-21.0	-5.3	-7.7	-16.2	-18.3	-14.7
Simulation (rc) [%]	-21.6	-18.5	-25.4	-35.7	-39.7	-37.1

6.3. Stresses

The test arrangement for the validation of wire stresses takes place with the help of the test bench shown in Fig. 22a, where the boundary conditions reported in Fig. 12 are implemented.

In a distance of 0.089 m to the clamp (the typical distance for bending amplitude measurements, [1]) strain gauges have been applied in axial direction of the individual outer wires. As the strain measurement was mainly done for comparison reasons, no measurements directly at the clamp have been performed. The evaluation of stresses at the clamp position is not practical, as they are influenced by the applied rigid boundary conditions and do not represent the real situation. The strain gauges capture the strains related on one hand on the wire tensile load and on the other those caused by wire bending. Fig. 23 shows the comparison between simulation and tests at the maximum deflection of

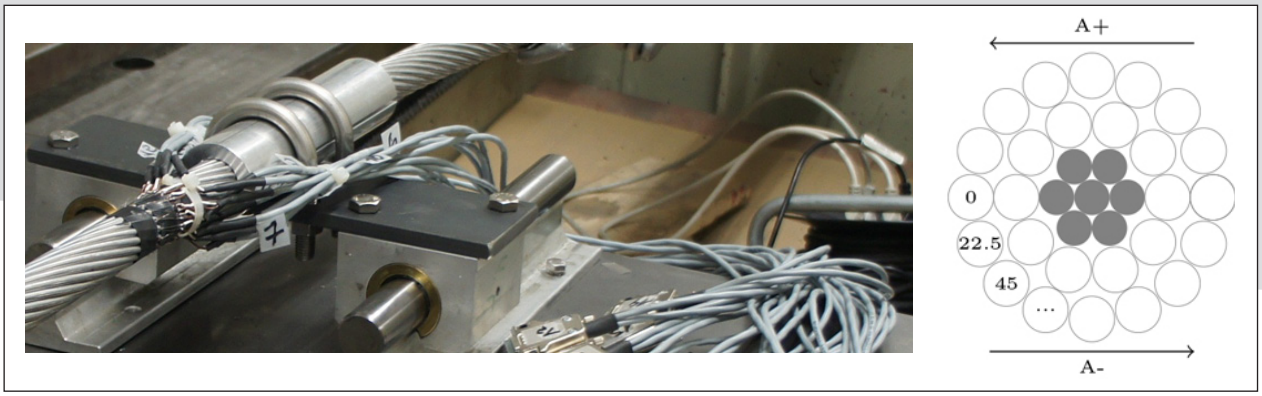

(a) Experimental setup

(b) Strain gauge positions (angular degree)

Fig 22. Strain measurement at ACSR Drake conductor.

0.02 m, whereby A+ and A- depict the positive respectively the negative displacement direction of the conductor, Fig.22b. As often with such measurements the results need a certain interpretation. The conductor wires show, due to the manufacturing process but also because of transport and storage on the drums, considerable deformations [16], which obscure the measured values of the local strains, but also the zeroing of the strain gauges. In order to exclude such undesirable effects, the conductor was slightly pre-tensioned and again released. The strain gauges were finally installed before tensioning at a minimum force to guarantee a straight stretched conductor. Fig. 23 presents only the stress values (measured strains are converted to stresses by using a Modulus of Elasticity of 57 GPa, Table I) appearing at maximum positive and negative deflection, i.e. caused by the bending process, the strains caused by the tensile load of 28.5 kN are not considered. The test results agree reasonably well with the simulation and also show the same curve shape as the analytical model [3].

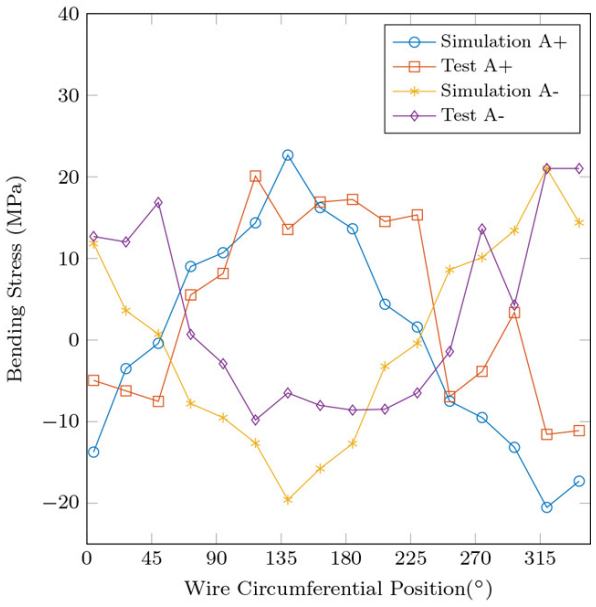

Fig. 23. Comparison of bending stresses at 0.089 m for ACSR Drake at max. mid-span deflection of 0.02 m.

7. Conclusion

This paper presents an efficient FE model for the numerical quasi-static simulation of overhead line conductors under simultaneous axial and bending loads. The results compare favorably with selected parameters accessible to analytical calculations but most importantly with carefully planned own experiments. As such tests are scarce, they may prove useful to other researchers for validating their own simulation tools. This new approach enables the modeling of relative long lengths of conductors allowing a better insight in the conductor bending process.

8. Acknowledgment

The authors gratefully acknowledge the financial support of this work by Swisselectric Research and the Pfisterer Sefag AG (Switzerland). Special thanks go to K.O. Papailiou for his encouragement on this work and the always valuable discussions with him on the subject of conductor bending.

9. References

[1] *EPRI Transmission line reference book: Wind-induced conductor motion, Palo Alto, CA, USA: EPRI, 2006.*

[2] *A. Cardou, "Stick-Slip Mechanical Models for Overhead Electrical Conductors in Bending," GREMCA, Université Laval, Québec, 2013.*

[3] *K.O. Papailiou, "Die Seilbiegung mit einer durch die innere Reibung, die Zugkraft und die Seilkrümmung veränderlichen Biegesteifigkeit," Ph.D. dissertation, Nr. 11057, ETH Zürich, 1995.*

[4] *K.O. Papailiou, "On the bending stiffness of transmission line conductors," IEEE Trans. Power Delivery, vol. 12, pp. 1576-1583, October 1997.*

[5] *S. Langlois, F. Legeron, F. Levesque, "Time History Modeling of Vibrations on Overhead Conductors With Variable Bending Stiffness," IEEE Trans. Power Delivery, vol. 29, pp. 607-614, 2014.*

[6] *C. Jolicoeur, A. Cardou, "Semicontinuous Mathematical Model for Bending of Multilayered Wire Strands," Journal of Engineering Mechanics, pp. 643-650, July 1996.*

[7] *R. Judge, Z. Yang, S.W. Jones, G. Beattie, "Full 3D finite element modelling of spiral strand cables," Construction and Building Materials, vol. 35, pp. 452-459, 2012.*

[8] *A. Nawrocki, M. Labrosse, T. Conway, "New specific finite element model for cables – Part I: Theory, " Proceedings of the Annual Convention of the Wire Association International, Atlanta, USA, pp. 95-113, 1999.*

[9] *R. Beleznai, I. Paczelt, "Design curve determination of two-*

layered wire rope strand using p-version finite element code," Engineering with Computers, vol. 29, no. 3, pp. 273-285, 2013.

[10] W. Zhou, H.-Q. Tian, "A novel finite element model for single-layered wire strand, " Journal of Central South University, vol. 20, no. 6, pp. 1767-1771, 2013.

[11] Y. Yu, X. Wang, Z. Chen, "A simplified finite element model for structural cable bending mechanism," International Journal of Mechanical Sciences, vol. 113, pp. 196-210, 2016.

[12] W. C. Young, R. G. Budynas, Roark's Formulas for Stress and Strain, Seventh Edition, McGraw-Hill, 2002.

[13] K. Feyrer, Wire Ropes, Heidelberg: Springer, 2007.

[14] C.B. Rawlins, Analytical Elements of Overhead Conductor Fabrication, Fultus Corporation, pp. 6-9, 2005.

[15] J.P. Paradis, F. Legeron, "Modelling of the free bending behavior of a multilayer cable taking into account the tangential compliance of contact interfaces," in ISCD 2011 Proc., 9th Int. Symp. on Cable Dynamics, Shanghai, China, October 2011.

[16] M. Frigerio, P.B. Buehlmann, J. Buchheim, S.R. Holdsworth, S. Dinser, Ch.M. Franck, K.O. Papailiou, E. Mazza, "Analysis of the tensile response of a stranded conductor using a 3D finite element model," Int. J. Mech. Sci., 106, pp. 176-183, 2016.

10. Biographies

Ralf Baumann studied Aerospace Engineering at the University of Stuttgart and graduated as Dipl.-Ing. in 1992. His employment experience includes several research and management positions at Hilti AG, Principality of Liechtenstein. In 2005 he moved to Lucerne University of Applied Sciences and Arts, Department Mechanical Engineering, as a lecturer for computational mechanics. Since 2006 he is Head of the Competence Center Mechanical Systems and received the professorship in 2007.

Pavel Novak studied Mechanical Engineering at the University of Applied Sciences and Arts in Lucerne and graduated as Bachelor of Sciences in 2010. Post-graduate he worked several years as an assistant and research engineer at the Competence Center Mechanical Systems. In 2014 he moved to Alstom as Tender Engineer. Since 2016 he is hired as Maintenance Engineer at Dectris.